EXPERIMENTAL AND COMPUTATIONAL INVESTIGATION OF ROTARY ELECTROMAGNETIC STIRRING IN A WOODS METAL SYSTEM

J. Partinen*, N. Saluja*, J. Szekely*, J. Kirtley Jr.**

*Department of Materials Science and Engineering
**Department of Electrical Engineering and Computer Science

Massachusetts Institute of Technology
77 Massachusetts Avenue, Cambridge, MA 02139-4307, USA

CONTENTS

ABSTRACT

An experimental and computational investigation was carried out in an electromagnetically stirred Woods metal system, and the associated free surface deformation was studied at various frequencies of the applied current. The free surface velocities were measured using high-speed video photography, and edge-effects of the electromagnetic stirrer were studied by varying the position of the melt relative to the electromagnetic stirrer. The calculated free surface deformation was compared to experimental observations made on a laboratory-scale installation.

INTRODUCTION

The beneficial effects of electromagnetic stirring in materials processing, especially in continuous casting, have been studied by many investigators. This research is well documented [1-6], and a sufficiently large data-base now exists to prove that though initially the cost of setting up the stirrer (capital costs, training personnel, and experimentation to determine optimum parameters) is considerable, the enhancement in quality and the flexibility achieved for varying certain operating parameters are very significant.

The use of a rotating magnetic field has been studied, but this research has focused mainly on the effect of stirring action on resulting microstructural modifications [7-10], or on rather simplistic theoretical models to predict the velocities and turbulence patterns inside the melt. One of the areas that has not received enough emphasis is the study of free-surface phenomena in melts that arise due to application of rotating electromagnetic fields. This free surface disturbance has a pronounced effect on the heat transfer and solute transport phenomena that cannot be neglected in the theoretical analysis of these systems. The altered flow patterns and turbulence conditions in the electromagnetically stirred melt manifest themselves in final product quality. Hence it is very important to address the phenomena of surface deformation and turbulence in the melt, with a sound theoretical basis complemented by intelligent experimental observations. In this paper, experimental investigation has been performed to determine the shape of the free surface. The theoretical model developed is used to track the free surface deformation with time, and the conformity of this model to experimental observations is analyzed.

EXPERIMENTAL RIG

The electromagnetic stirring device consists of an coil, shown in Figure 1, wound in a helical pattern [11]. In addition, the electrical system is composed of two transformers, a variable frequency drive to alter the frequency of the current applied to the stirring coil, and instrumentation for temperature measurement. A schematic description of the stirring system is presented in Figure 2.

The current from the power supply (60 Hz, three-phase, 100 A maximum, 220 V phase-to-phase voltage) is stepped up and fed to the variable frequency drive which outputs a current of adjustable frequency (2 - 60 Hz, 460 V maximum, three-phase.) The ratio of the output voltage and frequency from the variable speed drive is also controlled to provide varying levels of power input to the electromagnetic stirrer.

The electromagnetic stirrer is rated at 60 kVA, and has a hollow core (diameter: 150 mm, height: 500 mm) where the melt containing crucible is placed. The dimensions of the stirrer are given in table 1. The maximum field produced by the armature with the current arrangement is about 0.045 tesla; this can be substantially increased by modification of the electrical set-up. For this system, the theoretical model estimates characteristic melt velocity of about 1 m/s, which is typically found in many industrial EMS applications.

The metallic melt used in the experiments is Woods metal, the properties of which are listed in Table 2 [12] . This melt is placed in a clay bonded graphite crucible. The measurements of the magnetic field on the inner and outer surface of the crucible (without the melt) prove that the field losses due to the wall thickness of the crucible are in the order of 2%, and have therefore been neglected.

The surface velocity measurements of the electromagnetically stirred melt are made using a high-speed video camera and a motion analyzer. A setting of 500 frames/second is selected to film the motion of spherical alumina particles floating on the surface. The distance of travel, arc of the path, and the frame speed are used to extract the surface velocities.

The free surface deformation is recorded by a measuring pin mounted on a movable platform. The measurement of the radial and

tangential components of the magnetic field is made with a Hall-probe and with a search coil.

MATHEMATICAL EQUATIONS AND COMPUTATIONAL TECHNIQUE

Fluid flow equations

The fluid flow equations can be represented by the continuity equation, the equations of motion, and the k-ε turbulence model.

Equation of mass conservation:

$$\frac{\partial u}{\partial r}+\frac{\partial w}{\partial z}+\frac{u}{r}=0 \qquad (1)$$

where u,v, and w are the velocities in the directions r,θ, and z respectively, for a cylindrical coordinate system.

Equation of motion in the radial direction:

$$\frac{\partial u}{\partial t}+u\frac{\partial u}{\partial r}+w\frac{\partial u}{\partial z}-\frac{v^2}{r}=-\frac{1}{\rho}\frac{\partial p}{\partial r}+G_r+f_r \qquad (2)$$

Equation of motion in the azimuthal direction:

$$\frac{\partial v}{\partial t}+u\frac{\partial v}{\partial r}+w\frac{\partial v}{\partial z}+\frac{uv}{r}=G_\theta+f_\theta \qquad (3)$$

Equation of motion in the axial direction:

$$\frac{\partial w}{\partial t}+u\frac{\partial w}{\partial r}+w\frac{\partial w}{\partial z}=-\frac{1}{\rho}\frac{\partial p}{\partial z}+G_z+f_z \qquad (4)$$

where p is the static pressure, ρ is density and t is the time. G_r, G_θ are the body accelerations due to electromagnetic forces and G_z is

the body acceleration due to gravity. In the above f_r, f_θ, and f_z represent the viscous accelerations given by following equations:

$$\rho f_r = -\left\{\frac{\partial \tau_{rr}}{\partial r} + \frac{\partial \tau_{rz}}{\partial z} + \frac{1}{r}(\tau_{rr} - \tau_{\theta\theta})\right\} \quad (5)$$

$$\rho f_\theta = -\left\{\frac{\partial \tau_{r\theta}}{\partial r} + \frac{\partial \tau_{rz}}{\partial z} + \frac{2\tau_{r\theta}}{r}\right\} \quad (6)$$

$$\rho f_z = -\left\{\frac{\partial \tau_{rz}}{\partial r} + \frac{\partial \tau_{zz}}{\partial z} + \frac{\tau_{rz}}{r}\right\} \quad (7)$$

The following equations give the stress terms in equations (5), (6) and (7). For a fluid of dynamic viscosity μ, the stresses are

Normal stress ($i \neq j$)

$$\tau_{ii} = -2\mu\left[R_i \frac{\partial u_i}{\partial x_i} + \xi_{ij}\frac{u_j}{x_j}\right] \quad (8)$$

Shear stress:

$$\tau_{ij} = -\mu\left[\frac{\partial u_j}{\partial x_i} + R_j \frac{\partial u_i}{\partial x_j} + \xi_{ij}\frac{u_j}{x_i}\right] \quad (9)$$

where

$$i, j \equiv r, \theta, z;\ R_r = R_z = 1;\ R_\theta = \frac{1}{r};\ \xi_{rz} = \xi_{\theta z} = 0; \xi_{r\theta} = 1 \quad (10)$$

The volume of fluid function F(r,z,t) represents the volume of fluid per unit volume and satisfies the following equation:

$$\frac{\partial F}{\partial t} + \left[\frac{\partial}{\partial r}(Fu) + \frac{\partial}{\partial z}(Fw) + \frac{Fu}{r}\right] = 0 \quad (11)$$

where

$$F \begin{cases} =1 & \text{cell full of fluid} \\ 0<F<1 & \text{free surface exists} \\ =0 & \text{void region} \end{cases}$$

Voids represent regions containing no fluid mass and have uniform pressure assigned to them. In a physical sense, voids represent regions filled with gas whose density is insignificant compared to the density of the fluid.

The Reynolds stresses are represented by the standard k-ε model and the dynamic viscosity coefficient is assumed to be a sum of the molecular (ν_M) and turbulent viscosities (ν_T):

$$\mu = \rho(\nu_T + \nu_M) \qquad (12)$$

The turbulent viscosity can be expressed as follows:

$$\nu_T = C_\nu \frac{k^2}{\varepsilon} \qquad (13)$$

where k is the turbulent kinetic energy and ε is the energy dissipation function. C_ν is an empirical constant (= 0.09 in our computations.)

Equation (14) gives the turbulent kinetic energy per unit mass:

$$\frac{\partial k}{\partial t} + u\frac{\partial k}{\partial r} + w\frac{\partial k}{\partial z} = P + D_k - \varepsilon \qquad (14)$$

where P is the shear production term and D_k is the diffusion term. The following equations define these terms:

$$P = C_K\left(\frac{\mu}{\rho}\right)\left[2\left(\frac{\partial u}{\partial r}\right)^2+2\left(\frac{\partial w}{\partial z}\right)+\left(\frac{\partial v}{\partial r}-\frac{v}{r}\right)\left\{\frac{\partial v}{\partial r}+\left(-\frac{v}{r}\right)\right\}+\left(\frac{\partial u}{\partial z}+\frac{\partial w}{\partial r}\right)\left(\frac{\partial u}{\partial z}+\frac{\partial w}{\partial r}\right)+\left(\frac{\partial v}{\partial z}\right)\left(\frac{\partial v}{\partial z}\right)\right] \quad (15)$$

$$D_k=\left[\frac{\partial}{\partial r}\left(v_q\frac{\partial k}{\partial r}\right)+\frac{\partial}{\partial z}\left(v_q\frac{\partial k}{\partial z}\right)+\frac{v_q k}{r}\right] \quad (16)$$

C_k is an empirical constant equal to 1.0 and v_q is diffusion coefficient defined by equation (17).

$$v_q = C_{mk}\left(\frac{\mu}{\rho}\right) \quad (17)$$

where C_{mk} is an empirical constant equal to 1.0.

The transport equation for the turbulence dissipation can be expressed as:

$$\frac{\partial \varepsilon}{\partial t}+\left[u\frac{\partial \varepsilon}{\partial r}+w\frac{\partial \varepsilon}{\partial z}\right]=\frac{C_{\varepsilon 1}\varepsilon P}{k}+D_\varepsilon-\frac{C_{\varepsilon 2}\varepsilon^2}{k} \quad (18)$$

where $C_{\varepsilon 1}$ is the coefficient of production and $C_{\varepsilon 2}$ is the coefficient of decay. P and D_ε are similar to the constants given by equations 14 and 15 respectively, obtained by replacing k by ε and C_{mk} with an other constant $C_{m\varepsilon}$ in these equations.

Electromagnetic equations

Using the Maxwell's equations and Ohm's law the electromagnetic force field can be calculated. Applying the magneto-quasistatic approximation we have the following equations:

Continuity of the magnetic flux:

$$\vec{\nabla}\cdot\vec{B} = 0 \quad (19)$$

Ampere's law:

$$\vec{J} = \vec{\nabla} \times \vec{H} \tag{20}$$

Faraday's law:

$$\vec{\nabla} \times \vec{E} = -\frac{\partial \vec{B}}{\partial t} \tag{21}$$

Ohm's law for moving media:

$$\vec{J} = \sigma\left[\vec{E} + \left(\vec{u} \times \vec{B}\right)\right] \tag{22}$$

where $\vec{E}$ is the electric field, $\vec{H}$ is the magnetic field strength, $\vec{B}$ is the magnetic flux density, $\vec{J}$ is the induced current density and $\vec{u}$ is the velocity vector.

The electromagnetic body force can be calculated from the following relationship:

$$\vec{F} = \vec{J} \times \vec{B} \tag{23}$$

The expression for the force terms used were according to Spitzer *et al.* [13].

Radial component of the electromagnetic force density:

$$F_r = -\frac{1}{8} B_0^2 \left(\omega - \frac{v_\theta}{r}\right)^2 \sigma^2 \mu_0 r^3 \tag{24}$$

Azimuthal component of the electromagnetic force density:

$$F_\theta = \frac{1}{2} B_0^2 \left(\omega - \frac{v_\theta}{r}\right) \sigma r \tag{25}$$

where B_0 is the amplitude of B_r inside the stirrer, σ is the electrical conductivity and μ_0 is the magnetic permeability. The electromagnetic acceleration terms G_r and G_θ can be calculated from the fact that the acceleration equals force density per unit volume of the melt.

Boundary conditions

The following boundary conditions were set in the calculations:
- symmetry about the centerline
- no slip at the walls
- tangential stresses at the free surface are set to zero

It is assumed that the velocity profile obeys the logarithmic law, the turbulence energy is proportional to the wall shear stress, and that the length scale is proportional to the distance from the wall.

The boundary conditions for k and ε are set according to the well-established power-law profile [14]

Numerical technique

The equations were solved using Flow-3D, a commercially available fluid dynamics package with free surface capabilities. The electromagnetic force routines were linked to the program to calculate the source terms in the equations of motion. The free surface interface tracking in Flow-3D is performed by using the volume of fluid (VOF) method [15]. This method is not capable of resolving details of the interface that are smaller than the mesh size.

The domain of calculation was chosen so that it contains the fluid body and the gas in the mold above the fluid. The cells initially occupied by gas are used to accommodate the free surface deformation. In the calculations, an axisymmetric mesh with 45

grids in the radial direction and 60 grids in the axial direction was used.

RESULTS AND DISCUSSION

The electrical characteristics of the input power of the stirrer, both at line frequency and low frequencies are depicted in Figure 3 a),b) and c). It can be seen that at line frequency the sinusoidal approximation for the theoretical model is valid, but the waveform gets distorted at lower frequencies.

Figures 4 and 5 depict the variation of the magnetic field components B_r and B_θ with relative axial position ΔZ along the stirrer. Position ΔZ refers to the distance from the top of the stirrer. The bell-shaped curves in these figures show that the field values have a maxima at the coil center, and the field strength tapers off towards the edges of the coil. Hence, an assumption of a constant field strength along the axis of the coil is somewhat erroneous. To take this into account in the calculations it is necessary to allow the variation of the field with coil depth. In addition the field variation at the edges of the coil (the "edge-effects") has significant ramifications on the secondary flow fields in the system. The gradients in the magnetic field cause an axial gradient in the electromagnetic flow field. Hence even though the primary flow pattern is in the azimuthal direction, another flow pattern in the axial plane (with *r*- and *z*- components of the velocity) is set up. In practice, this axial flow field is very important because it enhances the effective 'stirring length' of the system. In other words, the stirring action occurs in a larger length of the system compared to the actual geometrical dimensions of the stirrer.

Figure 6 shows the temperature measurements with time without stirring, and for two different stirring frequencies. The temperatures were measured along the crucible axis, 1 *cm* from the bottom of the melt pool. The overall decrease in the melt temperature is due to the loss of heat from the top of the crucible as well as from the crucible sides. No compensation is made for these heat losses in the present system. Initially in the stirred melt, the temperature decrease is rapid both due to higher gradients and due to a sudden increase in surface area caused by surface deformation. However, the rate of temperature drop decreases with time due to Joule heating.

Figure 7 illustrates the free surface deformation of the metal at line frequency with different relative positions Z of the melt with respect

to the coil. The relative position of the crucible determines the effective magnetic field strength and hence the electromagnetic forces that drive the melt. Hence the surface deformation is a strong function of the positioning of the crucible, and the type of gradients in magnetic field which are in turn determined by the coil design of the stirrer. Figure 8 shows the measuring technique and the expressions $\Delta C, \Delta W, \Delta H$ and Z.

The effect of the bulk temperature of the Woods metal on the free surface deformation is shown in Figure 9. It is found that there is a sudden decrease in the surface deformation below a temperature of approximately 93° C. It should be noted that the melting temperature of the Woods metal is ~ 70° C. This is a clear indication that for experiments with molten Woods metal, monitoring and control of temperature is important because of thermal dependence of its properties.

Figure 10 is a photograph obtained in a particular frame by high speed video, taken at a speed of 500 frames per second. The location of the alumina particles are recorded, and the surface velocities are extracted from this data.

Figure 11 gives the time dependence of the surface velocity. The time "zero" refers to the moment of turning the stirring on. The surface deformation is quite remarkable at line frequency, and this causes some scatter in the velocity measurements due to the curvature of the free surface.

The absence of atmosphere control in the present set-up means that a presence of a surface scale is inevitable since the Woods metal oxidizes in air. The entrapment of alumina particles in the surface scale also affects the velocity measurements. Figure 11 shows the surface velocities for two different axial positions of the melt relative to the stirrer, and hence for different magnetic field strengths.

Figure 12 shows the comparison of the theoretically predicted free surface deformation with that obtained by experimental observations. It can be seen that the agreement obtained is quite good.

The theoretical model used above is very useful but does require refinements to incorporate effects of heat transfer, solidification, non-Newtonian effects, Joule heat generation, and development of

more robust turbulence models to study free-surface turbulence. The current model is shown to provide good understanding of the system behavior and furnish reasonably good estimates of free surface deformation.

CONCLUSIONS

The present work is aimed at providing a better understanding of the coupling between free surface phenomena and electromagnetic parameters in an electromagnetically stirred system. A better theoretical understanding is provided by including free surface and electromagnetic capabilities in the hydrodynamic model. The predictions made by this model compare well with the experimental results generated in a laboratory scale equipment. In addition to the free surface phenomena, the study provides insight into the effect of relative placement of the stirrer with respect to the melt. In most EMS systems, the aim is to achieve more vigorous mixing and shearing of dendrites, together with a relatively quiescent free surface. This work gives some rather important guidelines to achieve that. The principle findings of this study can be summarized as:

1. The free surface deformation can be significantly reduced by altering the position of the melt relative to the stirrer.
2. The coil design of the stirrer determines the 'map' of variation of magnetic field density, which significantly alters the free surface deformation.
3. The successful stirring of the Woods metal at large solid fractions effectively proves the utility of such EMS systems for rheocasting and compocasting applications.
4. Stirring at low frequencies, necessitated by the presence of a metallic mold between the melt and the coil, requires a more rigorous mathematical model for the prediction of flow patterns. This is because of the significant distortion of the originally sinusoidal waveforms of coil current.
5. The theoretical model presented here can be extremely useful in predicting the free surface deformation in many EMS applications.
6. For higher stirring power, used primarly to obtain higher bulk velocities, the free surface deformation is more pronounced. To minimize this deformation, the stirrer has to be intelligently positioned. Further, the use of auxiliary devices such as electromagnetic brakes and screens may be beneficial. Such devices have to be located close to the free surface to damp the velocities in its vicinity.

ACKNOWLEDGEMENTS

The authors would like thank Dr. Wayne Hagman of the Dept. of Electrical Eng. and Computer Science, MIT, for his help in fabrication of the experimental apparatus. We would also like to thank Dow Corning Corp. for donating silicone oil coolant for the stirrer, and Dr. James Sicilian of Flow Science Inc. for his valuable suggestions during the course of this work.

SYMBOLS

u,v,w :	velocities
r,θ,z :	directions in the cylindrical coordinate system
p :	static pressure
t :	time
ρ :	density
G_r :	Body accelerations due to
$G\theta$:	electromagnetic forces
G_z :	Body acceleration due to gravity
$fr,f\theta,f_z$:	viscous accelerations
μ:	dynamic viscosity
τ_{ii}, τ_{ij}:	normal and shear stresses
i,j:	indecies refering to r,θ and z
ν_M, ν_T :	molecular and turbulent viscosities
ε :	energy dissipation function
k:	kinetic energy
C_V:	empirical constant (= 0.09)
P :	shear production term
D_k, D_ε :	diffusion terms for k and ε
C_k :	empirical constant (=1)
ν_q:	diffusion coefficient
C_{mk} :	empirical constant (=1.0)
$C_{\varepsilon 1}$:	coefficient of production
$C_{\varepsilon 2}$:	coefficient of decay
$C_{m\varepsilon}$:	constant
$\vec{E}$:	electric field
$\vec{H}$:	magnetic field strength
$\vec{B}$:	magnetic flux density
$\vec{J}$:	induced current dencity
$\vec{u}$:	velocity vector
$\vec{F}$:	the electromagnetic body force
B_0:	amplitude of B_r inside the stirrer
B_r:	r component of the induced magnetic flux dencity
σ :	electrical conductivity
μ_0:	the magnetic permeability
F_r:	radial component of the electromagnetic force density
F_θ:	azimuthal component of the electromagnetic force density:
ΔZ:	axial position within the stirrer
Z,ΔC,ΔW,ΔH:	dimensions as explained in Figure 8

REFERENCES

[1] E. D. Tarapore and J. Evans: *Metall. Trans. B*, **7B** (1976), 343.

[2] H. S. Marr: *Iron Steel Int.*, **51** (1978), 87.

[3] K.H. Tacke and K. Schwerdtfeger: *Stahl und Eisen*, **99** (1979), 7.

[4] K. H. Spitzer, K. H. Tacke and K. Schwerdtfeger: Proc. Symp. Metallurgical Applications of Magnetohydrodynamics, Trinity College, Cambridge (1982).

[5] H. K. Moffat: *ZAMM*, **58** (1978), T65.

[6] J. P. Birat and J. Chone: *Ironmaking Steelmaking*, **10** (1983), 269.

[7] P.A. Davidson: *Materials Sci. and Tech.*, **1** (1985), 994.

[8] H.S. Marr: Proc. Symp. Metallurgical Applications of Magnetohydrodynamics, Trinity College, Cambridge (1982). Proc. Conf. on "Metallurgical Applications of MHD" (1982), 143.

[9] L. Beitelman, J. A. Mulcahy, R.Hadden, M.W. Bates, D.Desrosiers: Continuous Casting of Steel, Proc. of the 2nd Process technology Conference, Vol 2, AIME, Chicago (Feb. 1981), 270.

[10] R. Alberny, J.P. Birat: Continuous casting of Steel, Proc. of an Int. Conf. in Biarritz, 31 May - 2 June 1976 France, The Metals Society, London, (1977), 116.

[11] P.L. Conley, J.L. Kirtley, Jr., W.H. Hagman, and A.H.M.S. Ula: IEEE Transactions on Power Apparatus and Systems, Vol. PAS-99, No. 4, pp1642-1651, July/August 1980.

[12] W.F. Hughes, F.J. Young: Electromagnetodynamics of fluids, John Wiley & Sons, NY, USA (1966).

[13] Karl-Heinz Spitzer, Mathias Dubke, Klaus Schwerdtfeger: *Metall. Trans. B*, 17B (1986), 119.

[14] Flow-3D manual, Flow Science,1988

[15] C.W. Hirt, B.D. Nichols: Volume of Fluid (VOF) Method for the Dynamics of Free Boundaries, J. Comp. Phys. 39, 201, 1981.

Table 1. Dimensions of the stirrer used in the experiments

Number of phases	3
Number of circuits	2 (in parallel)
Number of turns/circuit	30
Winding form	Helical
Inner diameter	150 mm
Outer diameter	249 mm
Active length	248 mm
Stator core inner diameter	279 mm

Table 2. Physical data of the fused metal used in the experiments

Composition	50Bi-25 Pb-12.5 Sn-12.5 Cd
Melting point	70 °C
Density	8.37×10^{3} kg m^{-3}
Molecular viscosity	2.29×10^{-3} kg m^{-1} s^{-1}
Electrical conductivity	9.0×10^{5} Ω^{-1} m^{-1}
Specific heat	1.255×10^{2} J kg^{-1} K^{-1}
Thermal conductivity	1.405×10^{1} J m^{-1} s^{-1} K^{-1}
Thermal expansion coefficient	$1.0 \times 10^{-4} K^{-1}$

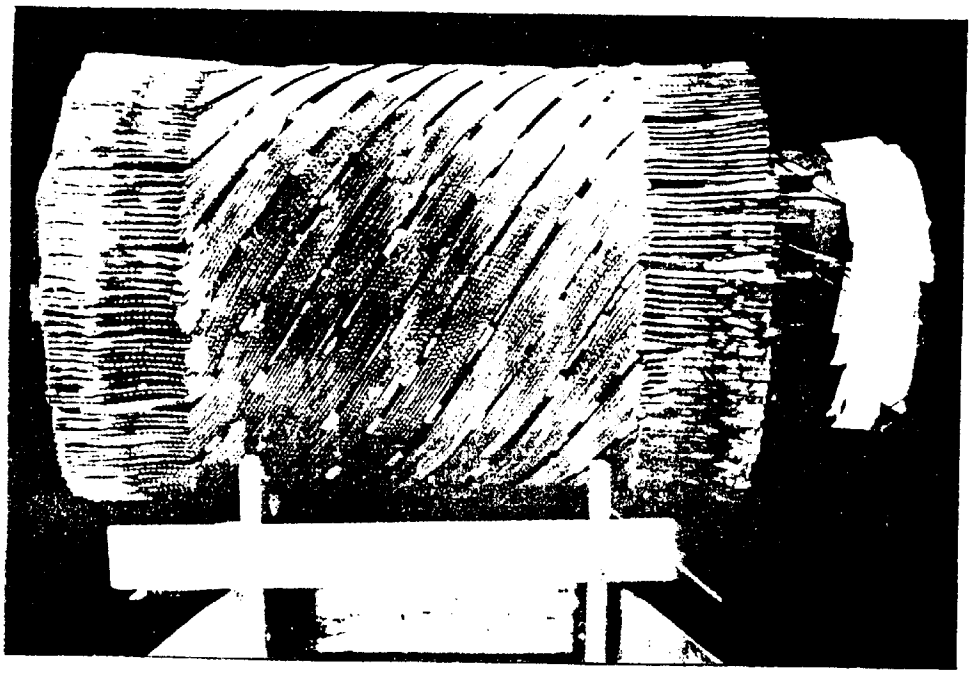

Figure 1. The armature with helical winding pattern

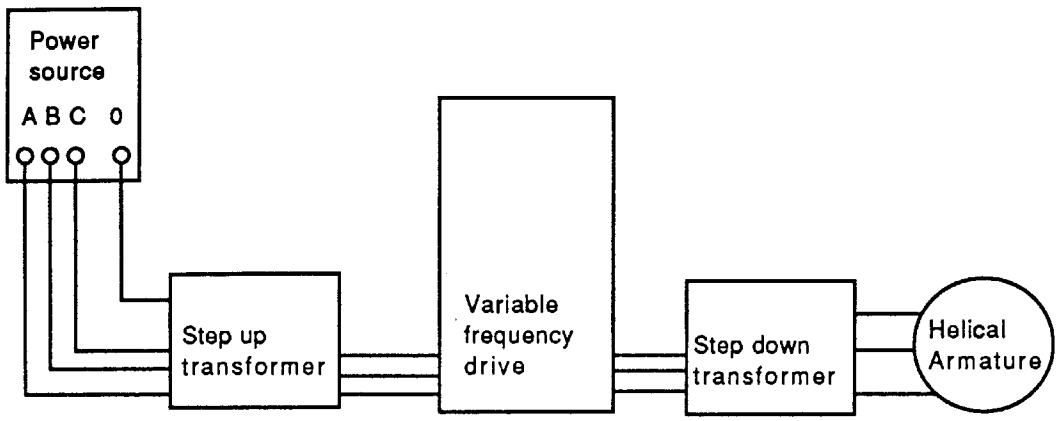

Figure 2. Schematic description of the stirring system

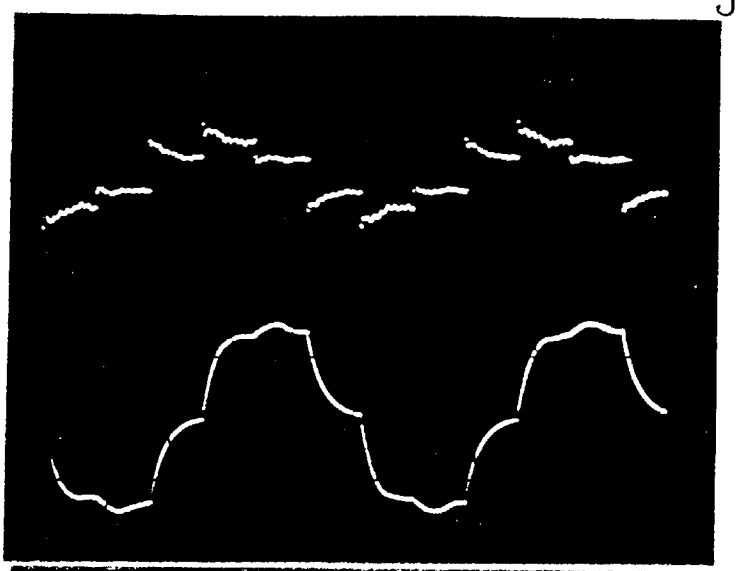

a) f=3.86 Hz

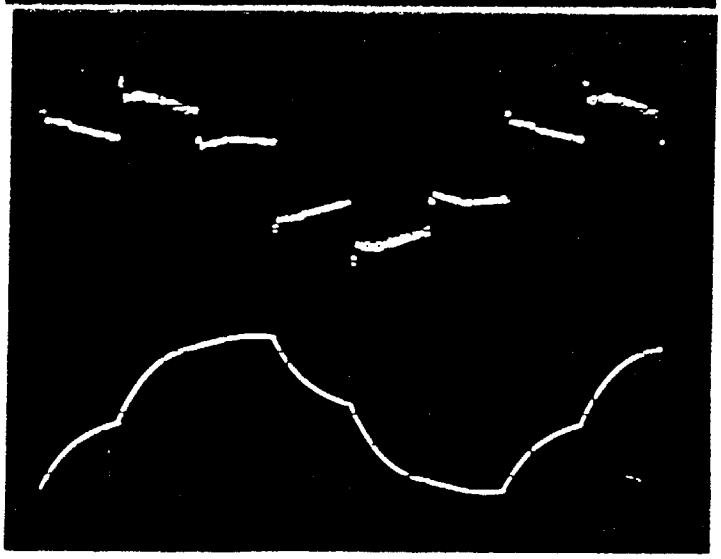

b) f=6.55 Hz

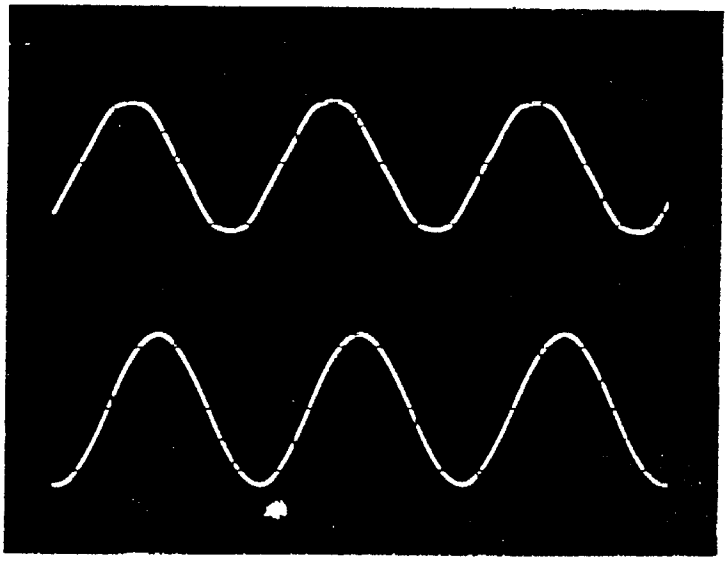

c) f=60 Hz

Figure 3. Voltage VAB(top) and current IA(bottom)waveforms at frequencies a) f=3.68 Hz,b) f=6.55 Hz, c) f=60 Hz

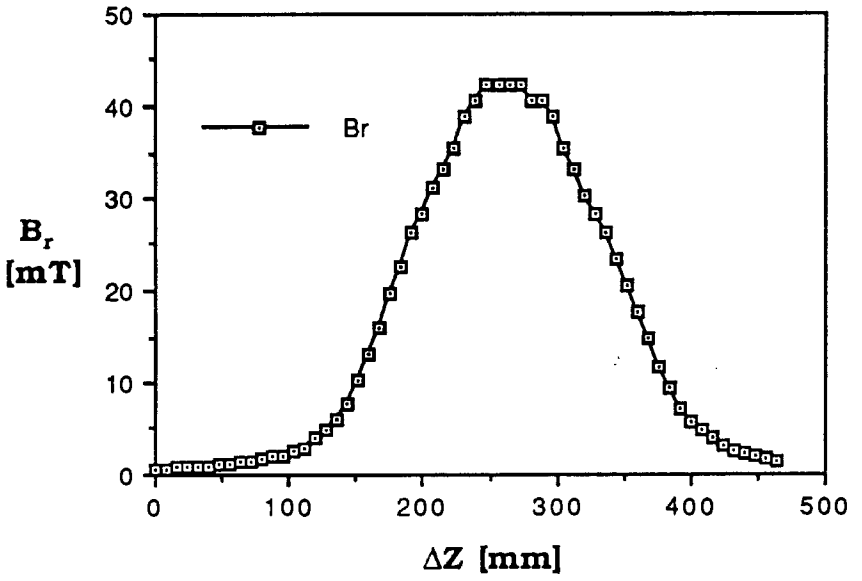

Figure 4. B_r vs axial position ΔZ within the stirrer

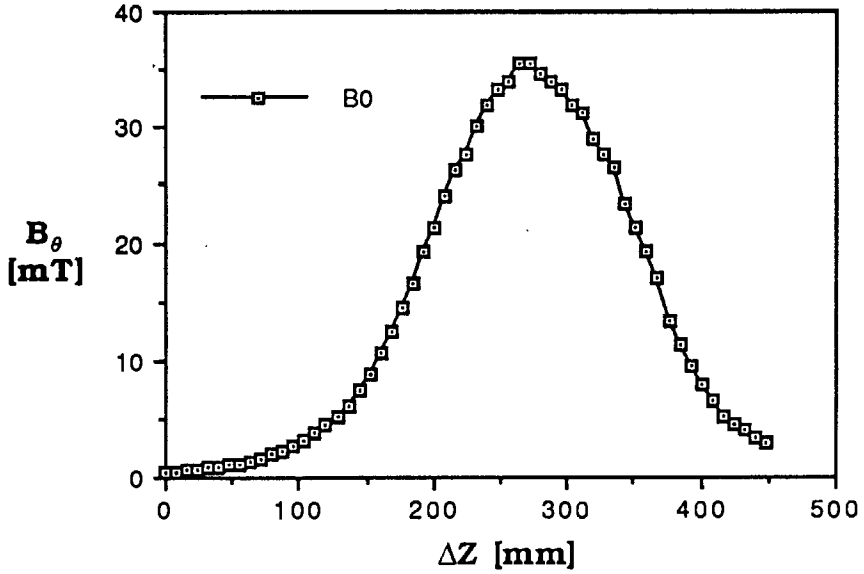

Figure 5. B_θ vs axial position ΔZ within the stirrer

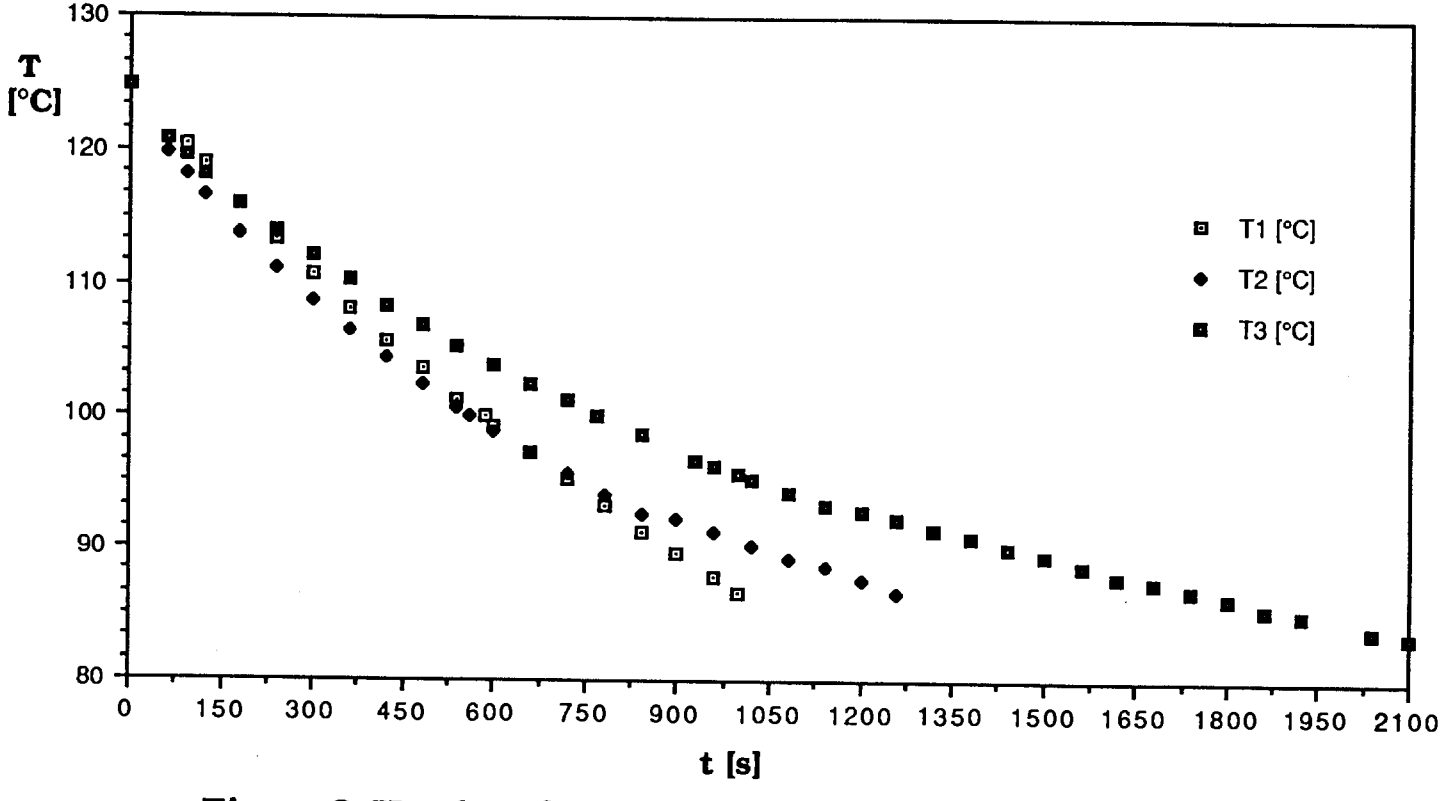

Figure 6. Heatloss from the melt without stirring and with two stirring frequencies. T1=0 Hz, T2=13,1 Hz and T3= 60Hz

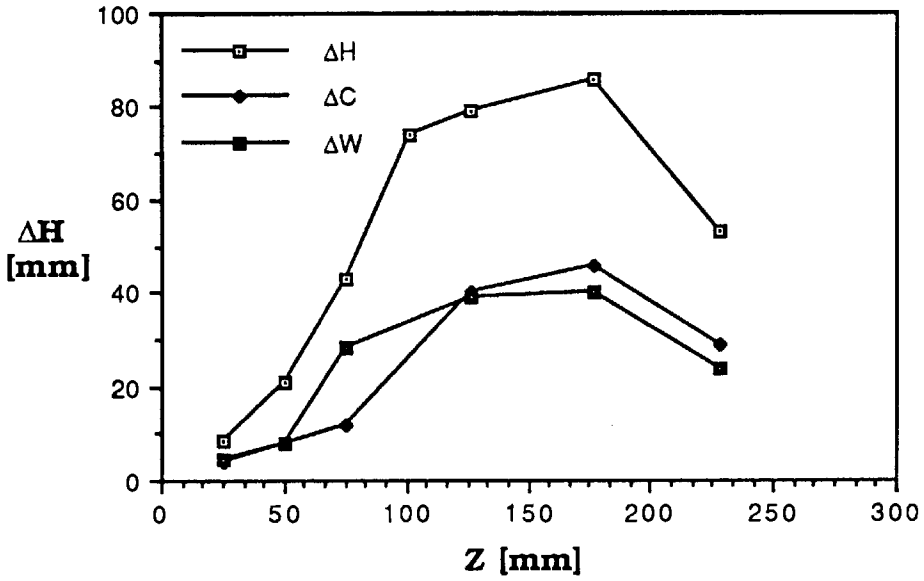

Figure 7. Free surface deformation vs axial position Z of the crucible

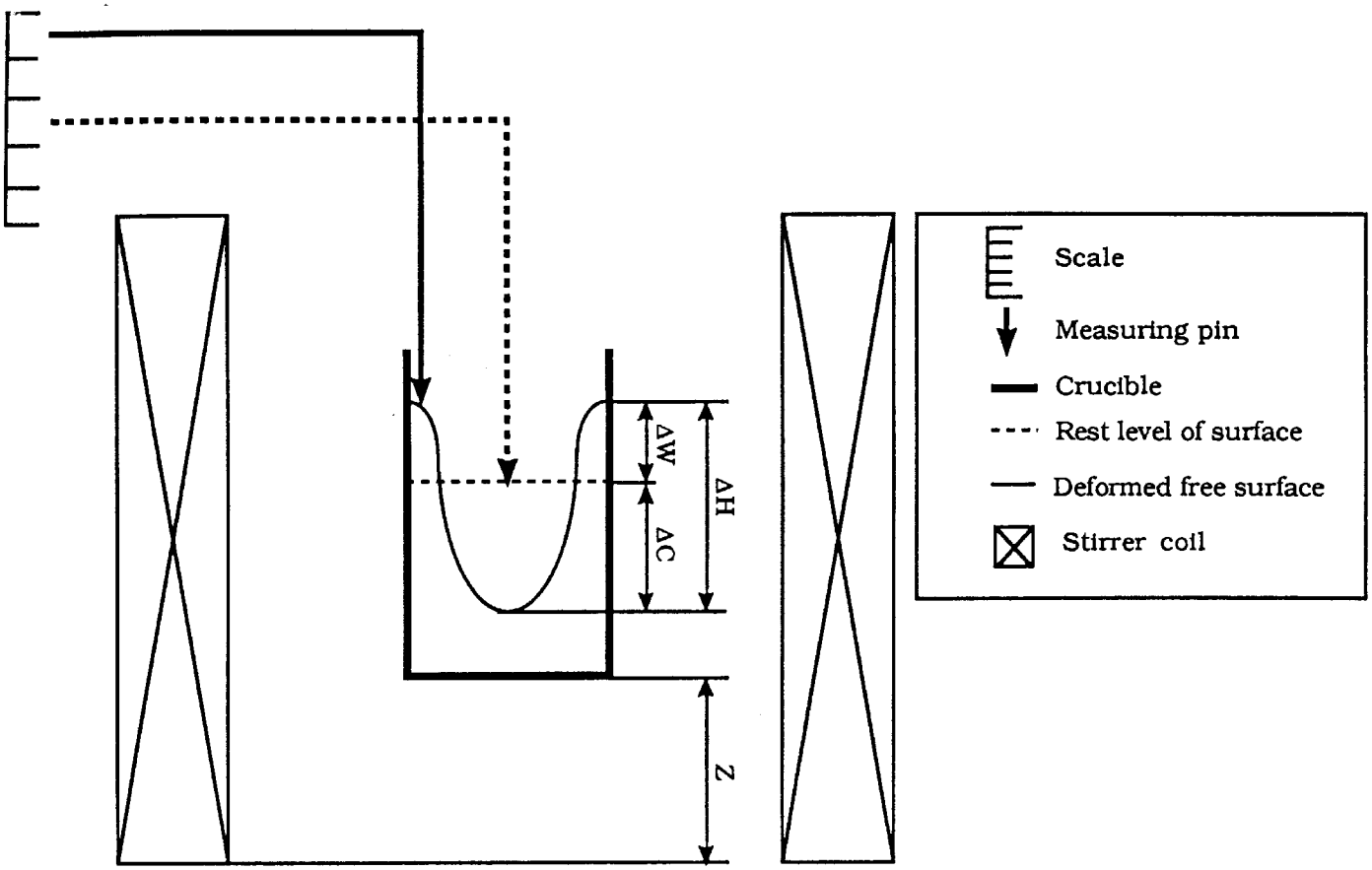

Figure 8. Measurement technique and physical meaning of ΔC,ΔW,ΔH and Z

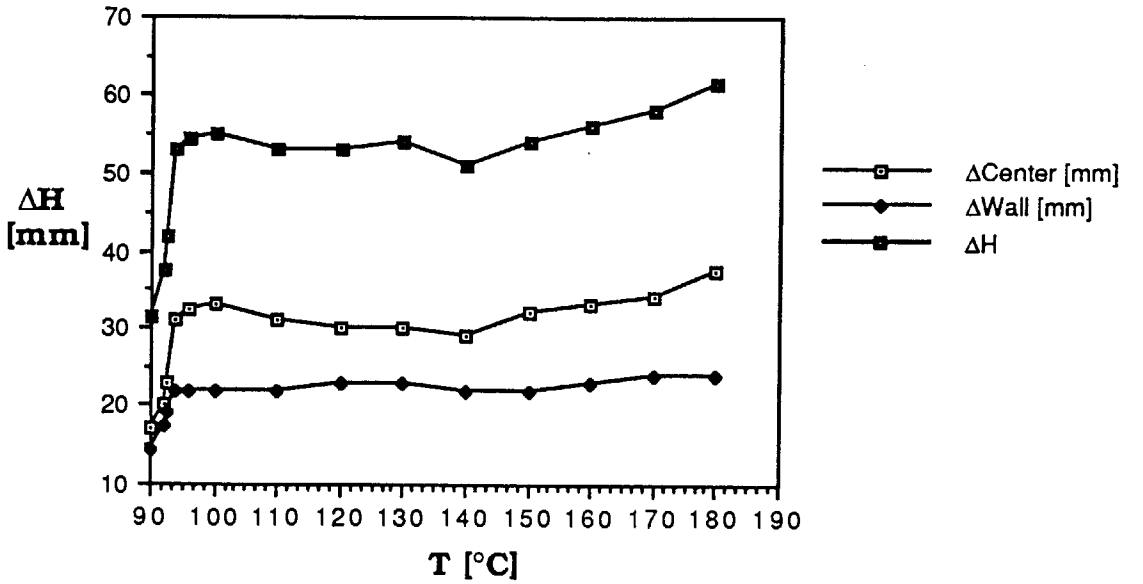

Figure 9. Dependence of freesurface deformation on temperature in Woods metal

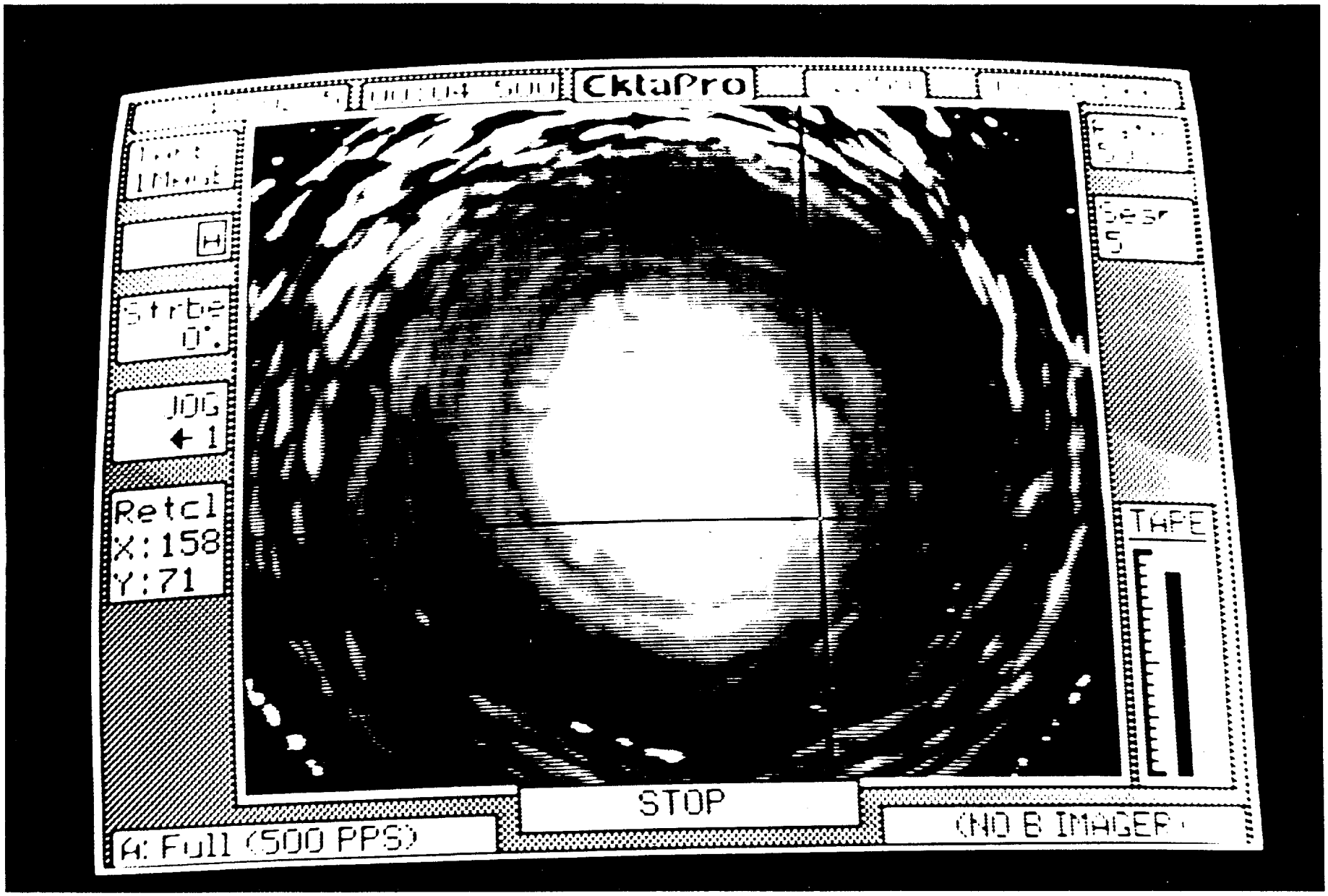

Figure 10. Photograph of a high speed video frame used for the surface velocity measurements

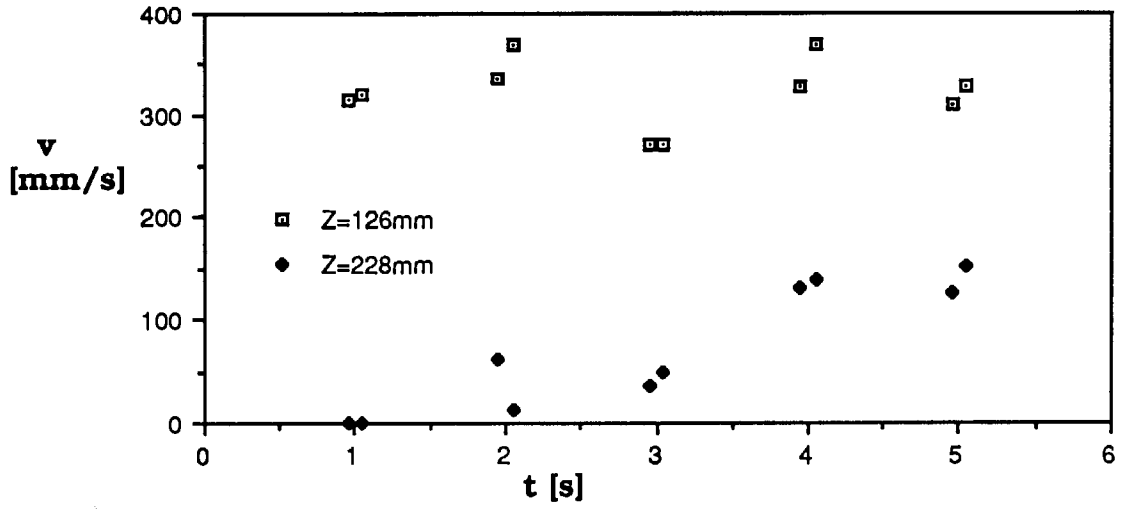

Figure11. Surface velocity at two different crucible locations

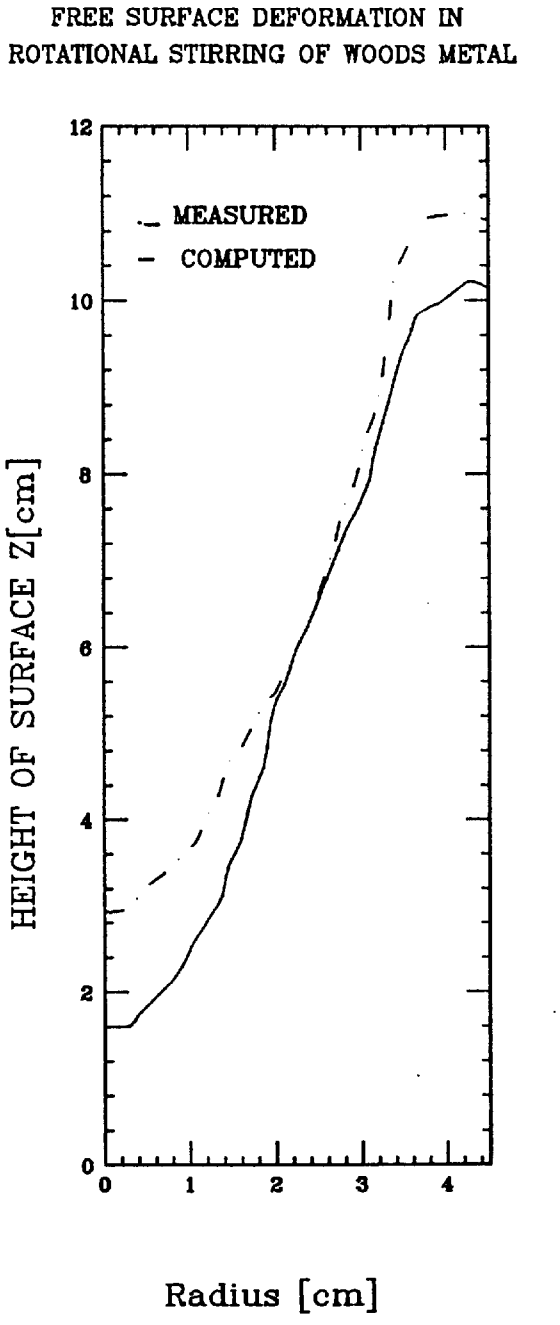

Figure 12. Predicted and measured free surface deformations in electromagnetically stirred woods metal system